Russian Chemical Reviews **81** (6) 549 – 559 (2012) © 2012 Russian Academy of Sciences and Turpion Ltd

DOI 10.1070/RC2012v081n06ABEH004287

Micro- and nanosized boron carbide: synthesis, structure and properties

R A Andrievski

Contents

I.	Introduction	549
II.	Synthesis	550
III.	Structure and properties	555
IV.	Conclusions	557

Abstract. Methods of synthesis of powder particles, fibres (wires), tubes, films, coatings and bulk materials based on micro- and nanocrystalline and amorphous boron carbide are considered. Specific features of the electronic structure, material structure and physicochemical and mechanical properties of boron carbide and boron carbide-based composites are discussed. Their existing and potential applications are highlighted. The little studied aspects of the research area in question are specified. The bibliography includes 105 references.

I. Introduction

Boron carbide have long attracted attention of chemists, physicists, materials scientists and other specialists owing to its low density, favourable hardness and elastic properties, high melting point and chemical inertness, as well as to specific nuclear and electric characteristics. In the last few years, the interest has increased because of much recent effort to create boron carbide-based armour, thermoelectric, semiconducting, biological and radiation-resistant materials (see, *e.g.*,[1–5]). It is of interest to consider how varying the structural parameters and going from common bulk crystalline materials to micro- and nanocrystalline materials change their physicochemical and mechanical properties and performance.

Using this scenario, we studied most of refractory compounds (carbides, nitrides and borides),[6] hydrides[7,8] and silicon carbide-based materials.[9] In this review, as well as in other works,[6–9] the terms micro- and nanosized are used with respect to both micro-and nanostructural (micro- and nanocrystalline) and micro- and nanoamorphous materials since many of boron carbide-based objects (particles and films) are prone to amorphization. The conventional boundary between 'micro' and 'nano' is taken to be at 100 nm, and the upper limit of 'micro' is at about 5×10^3 nm.

The properties of boron carbide have been studied for a long time (see, *e.g.*,[10–16]); however, many of its specific features are still debatable, which is explained by a variety of preparation methods and difficulties of phase certification of samples. The most frequently encountered variants of the phase diagram of the B–C system are shown in Fig. 1. The first variant (Fig. 1 *a*) is based on the generalization of results of many studied, including the refinement of the composition of boron carbide with the limiting carbon content and the congruent melting composition.[16] The diagram has a wide homogeneity range of boron carbide at the centre (deviations from the stoichiometric composition are considerable: ranging from ~9 at.% to ~24 at.% C). This phase diagram is accepted as the most reliable one by many researchers (see, *e.g.*, Refs 10 – 12, 15).

The second variant of the B–C phase diagram (Fig. 1 *b*) implies the existence of the $B_{13}C_{2\pm x}$ phase with a narrow homogeneity range up to ~800 °C and hyperstoichiometric compositions at higher temperatures, as well as other boron carbide phases (from $B_{51}C$ to $B_{13}C_3$).[17]

A calculated B–C diagram was recently reported at the 17th International Symposium 'Boron, Borides and Related Compounds' (ISBB 2011, Istanbul, 2011). According to this phase diagram, the rhombohedral boron carbide modification with a wide homogeneity range (from ~9 at.% to ~24 at.% C) exists only at high temperatures, whereas at $T < 600$ K peritectic decomposition leads to the monoclinic B_4C modification with a narrow homogeneity range.[18] The B–C diagram variants reported in studies[17,18] are very credible, but require further detailed experimental verification.

Most of commercial boron carbide products are formulated as B_4C ($B_{12}C_3$). Other formulas are also encountered, for example, $B_{13}C_2$ or B_7C_2, which describe, respectively, the hyperstoichiometric and hypostochiometric (with respect to B_4C) phases formed due to structural vacancies. Selected physicochemical characteristics of the most common boron carbide compositions are summarized in Table 1.

R A Andrievski Institute of Problems of Chemical Physics, Russian Academy of Sciences, prosp. Akad. Semenova 1, 142432 Chernogolovka, Moscow Region, Russian Federation. Fax (7-496) 522 35 07, tel. (7-496) 522 77 93, e-mail: ara@icp.ac.ru

Received 9 November 2011
Uspekhi Khimii **81** (6) 549 – 559 (2012); translated by G A Kirakosyan

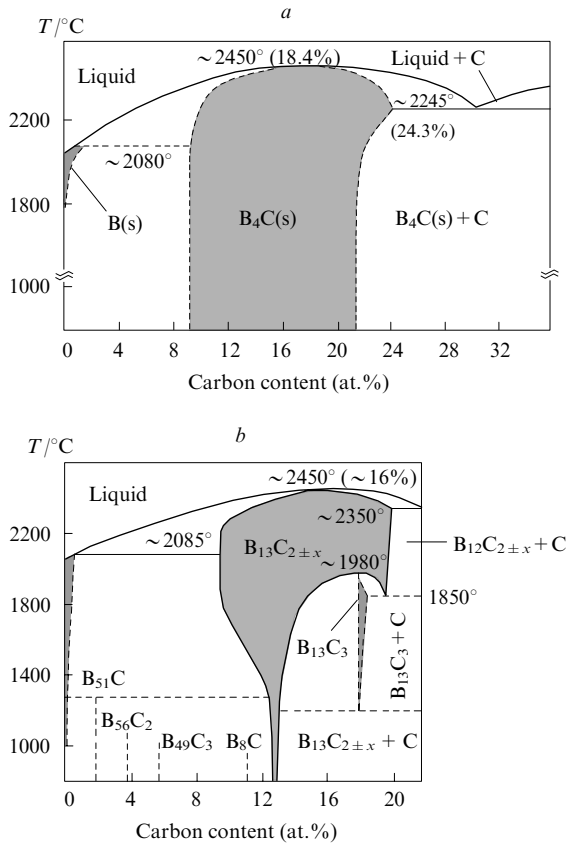


Figure 1. The most frequently encountered variants of the phase diagram of the B–C system with a wide homogeneity range of the B_4C solid modification (*a*) and with a narrow homogeneity range of $B_{13}C_{2\pm x}$ extended at high temperatures (*b*).[4]

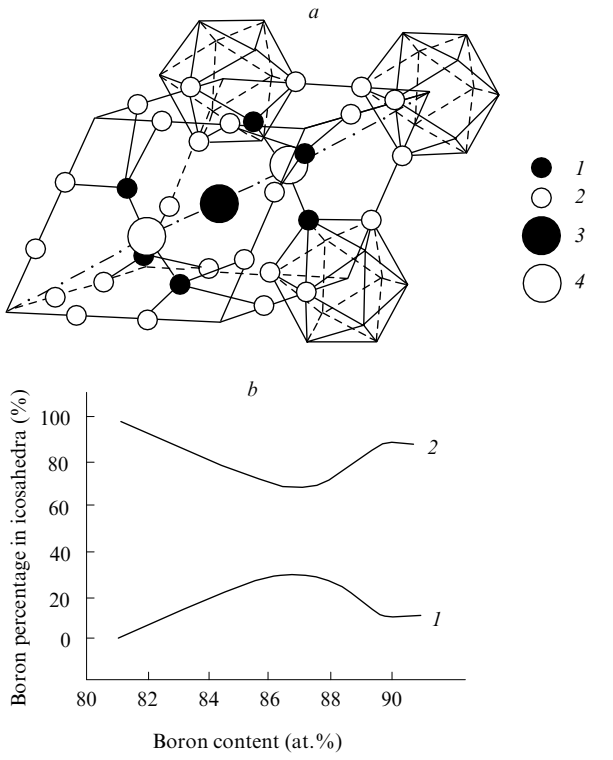


Figure 2. Rhombohedral unit cell of boron carbide with $B_{11}C$ icosahedra (*a*) and the effect of the boron content on the filling of its sublattice in B_{12} and $B_{11}C$ icosahedra (*b*).[13, 14]
(*a*) (*1*, *2*) Boron atoms in the h_1 and h_2 positions, respectively; (*3*) boron atoms in the 1*b* positions; (*4*) carbon atoms in the 2*c* position; (*b*) (*1*) for the B_{12} icosahedron; (*2*) for the $B_{11}C$ icosahedron.

Table 1. Selected physicochemical characteristics of the most common boron carbide compositions.

Parameter	B_4C	$B_{6.5}C$	Ref.
Structure	rhombohedral	rhombohedral	12
Space group	*R*3*m*	*R*3*m*	12
Unit cell parameters /nm			
a	0.5598	0.5630	12
b	1.2120	1.2190	12
Density /g cm^{-3}	2.52	2.46, 2.488	12, 13
Carbon content (at.%)	20	13.33	10–12
T_m /K	2620–2740	—	10
	—	2730	12
	2720	~2670	14
Vickers hardness /GPa	48.5	37	14
Shear modulus /GPa	198–205 [a]	185–195	15
Electric resistance /Ω m	10^{-3}–10^{-1}	$\sim 8\times10^{-4}$	12, 14
Band gap width /eV	1.64	—	12
TLEC [b] (300–1100) /K^{-1}	4.5×10^{-6}	5.5×10^{-6}	12

[a] For the $B_{4.3}C$ composition. [b] Thermal linear expansion coefficient.

'Building blocks' of the rhombohedral unit cell of boron carbide are B_{12} or $B_{11}C$ icosahedra located at its vertices and joined by the C–C–C or C–B–C chains along the major diagonal (Fig. 2*a*). Figure 2*b* shows how the filling (defectiveness) of the boron sublattice changes as a function of boron concentration. It is believed that variation of the concentration of structural vacancies in the homogeneity range is one of the crucial factors determining the evolution of physicochemical properties within this range. The change in the hardness, lattice constant, thermal and electrical conductivity, as well as thermoelectric characteristics, depending on the carbon content within the composition range $BC_{3.5}$–$BC_{6.0}$ (including the effect of the isotope composition) has been comprehensively covered.[13, 14, 19]

II. Synthesis

1. Micro- and nanopowders, nanowires and nanotubes

Boron carbide powders for manufacturing abrasives and for other applications are produced by many companies [for example, OOO Liprom (Russia), OAO Zaporozhabraziv (Ukraine), H C Starck Company (Germany) and others]. One of the finest commercial technical powders (H C Starck Company) has an average particle size of ~3 μm (F1200). This company also produces finer fractions of special purity (HD20; average particle size, 0.5 μm; specific surface area, 22–27 m^2 g^{-1}; B : C = 3.7–3.9), which are used for creating sintered materials for different purposes.

Boron carbide is synthesized by different methods: direct synthesis from elements, carbothermic reduction of boron oxide, metallothermic reduction of boron oxide with

magnesium in the presence of carbon, various versions of gas-phase interaction. The following methods of producing micro- and nanopowders, nanowires, nanotubes and fibrous and porous nanostructures based on boron, carbon and boron carbide have been described:

— synthesis from initial B and C nanopowders in a hydrogen atmosphere at relatively low temperatures (1123 – 1473 K), which yields hollow and fibrous nanostructures; [20]

— synthesis from initial amorphous B and C powders in an argon atmosphere at 1823 K, which yields powders with a particle size within 15 – 350 nm (average particle size ~200 nm; [21]

— carbothermal synthesis from a mixture of boron oxide and amorphous carbon in a vacuum at 1573 – 1773 K, which yields a mixture of crystalline and amorphous B_4C powders with a bimodal size distribution, ~70 nm and ~260 nm.[22] An analogous carbothermal synthesis has been used for obtaining nanostructural B_4C coatings on diamond powders in an argon atmosphere (T = 1423 K); [23]

— low-temperature synthesis of boron carbide in an argon atmosphere (T = 1523 – 1573 K) from a mixture of boric acid and glycerol calcined (in air at 823 K), which yields a boron carbide powder with an average grain size of ~1.1 μm and a low content of residual carbon; [24]

— combination of the synthesis from initial components with compaction by the pulsed electric current sintering method at pressure P = 20 MPa and a stepwise increase in temperature from 1573 to 2173 K, which yields $B_{13}C_2$ compacts with a relative density of 95% and a grain size of ~410 nm; [25]

— gas-phase synthesis from boron halides, carbon tetrachloride, hydrocarbons like CH_4, C_2H_2 and C_3H_8, as well as B and B_2O_3 evaporation products, which affords nanowires, nanofibres, nanosheets and nanobelts. For this purpose, plasma-activated processes, laser evaporation, catalysts, carbon nanotubes, polymer precursors and special templates are used (see, *e.g.*, Refs 1, 26 – 31);

— autoclave synthesis (T = 873 K, t = 8 h) from amorphous boron powders and liquid CCl_4 with lithium metal as a reducing agent, which yields nanocrystalline boron carbide powders with a grain size of 15 – 40 nm; [32]

— synthesis of micropowders based on compounds in composite systems like Ti – B – C and Si – N – C – B by means of intense mechanical grinding of mixtures of intial compound powders ($B_4C + TiO_2 + C$ and $BN + C + Si$, respectively), which are then compacted by the pulsed electric current sintering method.[33, 34]

Scanning electron microscopy (SEM) images of boron carbide nanoparticles, nanowires, nanosheets and nanobelts are shown in Fig. 3. As is seen, the morphology of nanosized forms is rather diverse. Single-crystal nanoparticles synthesized by reactions of boron vapour, obtained from decomposition of magnesium diboride, with carbon nanotubes (T = 1423 K) are faceted (Fig. 3 *a*). Nanoparticles form at the ends of nanotubes (Fig. 3 *b*),[26, 27] as well as at defects.[26] The size distribution of nanoparticles is lognormal, including bimodal forms.[22] The length of nanowires 10 – 100 nm in diameter (as a rule, the average diameter is ~50 nm) is several hundreds of nanometers, but can be as large as a millimeter.[28]

In addition to crystalline and amorphous boron, boric acid and boron oxide are used as the initial components in synthesis of boron carbide. When heated, these compounds undergo the following transformations: at T = 373 – 443 K, orthoboric acid (H_3BO_3) converts into metaboric acid (HBO_2) melting at ~510 K to form the B_2O_3 oxide, which melts at T > 750 K (the boiling point is above 1950 K).[23] Taking into account these data, basic reactions of numerous versions of the synthesis of nanosized boron carbide can be written in general form as follows: [28]

$$B_2O_3(l) \longrightarrow B_2O_3(g) \quad (1)$$

$$C(s) + B_2O_3(l) \longrightarrow B_2O_2(g) + CO(g) \quad (2)$$

$$8\,CO(g) + 2\,B_2O_3(g) \longrightarrow B_4C(s) + 7\,CO_2(g) \quad (3)$$

$$6\,CO(g) + 2\,B_2O_2(g) \longrightarrow B_4C(s) + 5\,CO_2(g) \quad (4)$$

$$7\,C(s) + 2\,B_2O_3(l, g) \longrightarrow B_4C(s) + 6\,CO(g) \quad (5)$$

Noteworthy are reactions involving oxygen impurities and water vapour in the furnace space.[30]

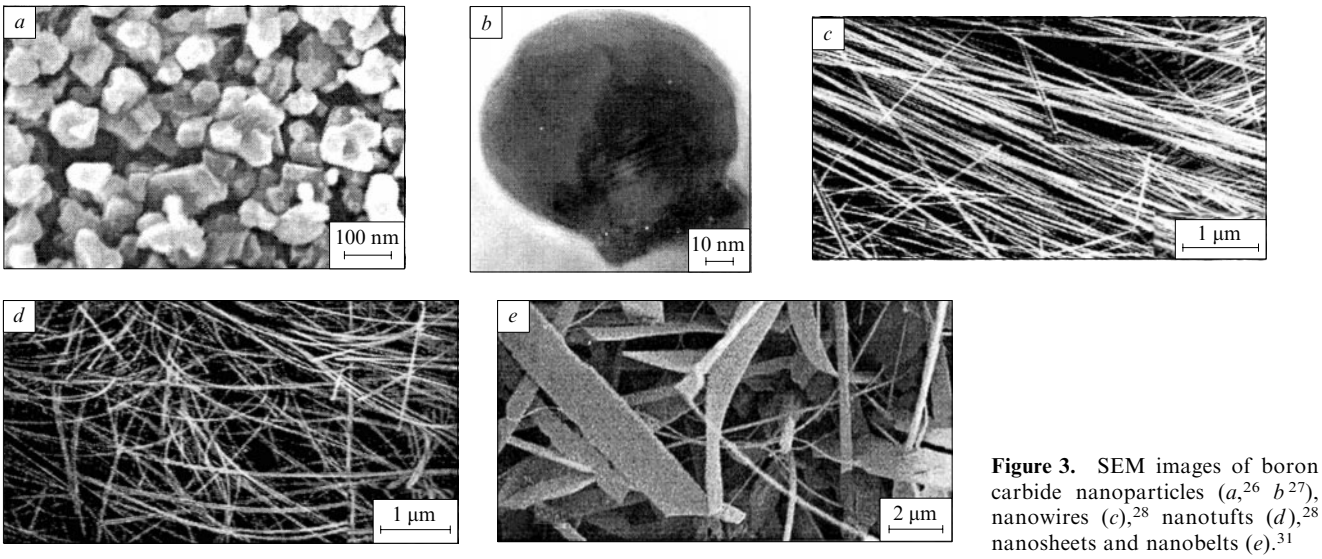


Figure 3. SEM images of boron carbide nanoparticles (*a*,[26] *b*[27]), nanowires (*c*),[28] nanotufts (*d*),[28] nanosheets and nanobelts (*e*).[31]

$$B(s) + (x/2)\,O_2 \longrightarrow BO_x(g) \quad (6)$$

$$B(g) + x\,H_2O \longrightarrow BO_x(g) + x\,H_2(g) \quad (7)$$

Judging by the character of reactions (1)–(7), gas-phase mass transfer plays a significant role in the synthesis of boron carbide.

It is suggested that nanowires are formed by the vapour–solid mechanism.[28] In the presence of catalysts (Ni or Fe), a liquid phase can form and other growth mechanisms (vapour–liquid–solid or solid–liquid–solid) are possible.[31] However, as far as is known, specific features of the carbidization kinetics and mechanism have been little studied. Electron microscopic study of nanowires of covalent carbides (B_xC, SiC) and interstitial carbides (TiC, TaC, NbC, Ti_xNb_{1-x}, Ta_xNb_{1-x}) revealed a general character of the carbothermal reductions in the presence of nickel and iron catalysts.[30]

Thermodynamic analysis of conditions of coating deposition on particles of diamond powders[23] showed that the carbide formation by the reaction

$$2\,B + 2\,H_3BO_3 + 7\,C \longrightarrow B_4C + 6\,CO + 3\,H_2 \quad (8)$$

begins at ~1670 K (Fig. 4), which is roughly consistent with experimental evidence. The distinction of the clearly nonequilibrium carbidization conditions from equilibrium thermodynamic estimates should also be taken into account. The morphology of resulting boron carbide nanostructures (Fig. 3) depends on the boron oxide vapour pressure [reactions (3)–(7)] and the effect of catalysts, as well as on the properties of the carbide and substrate surfaces; as far as is known, the role of these factors has not been considered theoretically so far.

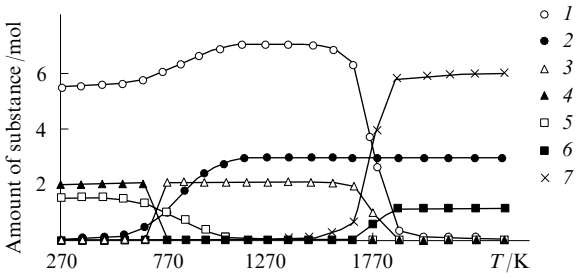


Figure 4. Influence of temperature on the amounts of components of reaction (8).[23]
(*1*) Carbon, (*2*) hydrogen, (*3*) B_2O_3(s), (*4*) CH_4, (*5*) B_2O_3(l), (*6*) B_4C, (*7*) CO.

Common methods for determining the size of nanostructures are X-ray diffraction, SEM, transmission electron microscopy (including high-resolution TEM) and measurement of the specific surface of powders by the Brunauer–Emmett–Teller method (see, *e.g.*, Refs 6 and 9). For studying carbon and oxygen impurities and phase analysis, X-ray photoelectron microscopy, Fourier transform Raman and IR spectroscopy, energy dispersive spectroscopy, electron energy-loss spectroscopy and Auger spectroscopy are used in addition to the above methods.

The X-ray powder diffraction pattern of a B_4C nanopowder obtained by the direct reaction of solid boron and carbon at 1823 K,[21]

$$4\,B + C \longrightarrow B_4C\,, \quad (9)$$

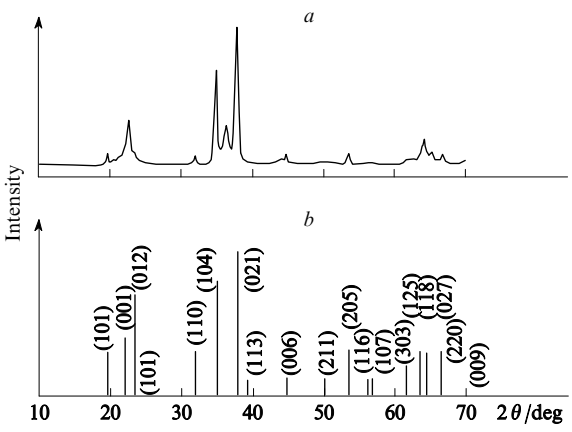


Figure 5. X-Ray diffraction pattern of B_4C nanopowder (*a*) and intensities of diffraction reflections (*b*) according to the data of the Joint Committee on Powder Diffraction Standards (No. 6-0555).[21]

is shown in Fig. 5. As demonstrated by TEM, some differences between the experimental and calculated data are caused by a small particle size (< 50 nm) of synthesized nanopowders and a high density of twin defects.

The B_4C and $B_{13}C_2$ carbides have identical crystal lattices with slightly different lattice constants. Nevertheless, they can be identified by X-ray crystallography, using the difference between the intensities of some reflections [for example, (012) and (104)] and their 2θ angles.[21,28]

X-Ray crystallography data are usually supplemented with the results of TEM and high-resolution TEM study. Figure 6 shows electron microscopy images of $B_{13}C_2$ samples obtained by the direct synthesis from boron and carbon powders coupled with compaction by the pulsed electric current sintering method.[25] The light-field image (Fig. 6*a*) indicates the presence of texture and the high density of parallel dark and light sheets inside separate grains, which is presumably caused by planar defects and amorphous interlayers. The typical dark streak pattern of a grain is observed at large magnifications (Fig. 6*b*).

Information on the homogeneity of composition in different nanoparticles can be obtained by means of electron energy-loss spectroscopy. In particular, from the results of determination of the boron and carbon contents

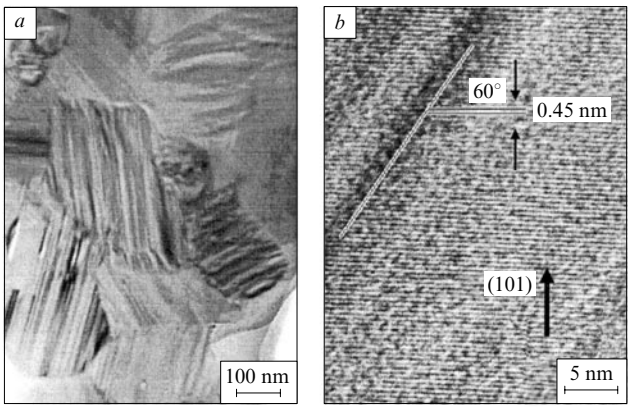


Figure 6. TEM images of nanograins in $B_{13}C_2$ samples obtained at different resolution.[25]

in 18 boron carbide nanoparticles obtained by the direct synthesis,[21] the average B : C ratio turned out to be 4.16 ± 0.48; approximately the same result was obtained in analysis of individual nanoparticles in other experiments.

For high-quality certification of nanoobjects, it is essential to use several independent methods of investigation (for example, X-ray crystallography, TEM, energy dispersive spectroscopy, energy-loss electron spectroscopy, *etc.*) in order to enhance the reliability of the results. An example of using different methods (X-ray crystallography, Raman spectroscopy, X-ray photoelectron microscopy, TEM, Auger spectroscopy and electron diffraction) for complex certification of nanopowders prepared by the reaction

$$4\,B + CCl_4 + 4\,Li \xrightarrow{873\,K} B_4C + 4\,LiCl,$$

has been considered.[32]

2. Films

The above information mainly concerns equilibrium powders and sintered and melted samples. The situation is complicated in the case of films: they are characterized by considerable nonequilibrium and an increase in the number of modifications of boron carbide and other compounds (see, *e.g.*,[33–35]). In particular, as applied to films obtained by chemical vapour deposition from the ($BCl_3 + CH_4 + H_2$) gas phase at 1303–1503 K and a pressure of 6.6 kPa, the phase diagram of the B–C system[33] contains four crystalline and two amorphous phases of boron carbide, although the existence of two-phase regions (a necessary attribute of two-phase systems) is debatable.[35]

In addition to chemical vapour deposition, physical vapour deposition methods are widely used to produce boron carbide films: magnetron sputtering in various regimes (DC, RF and pulsed DC),[36–43] pulsed-ion beam evaporation and laser physical vapour deposition,[2,44] air plasma spraying[45] and other methods. The pulsed-ion beam evaporation method enables the fabrication of crystalline $B_{13}C_2$ films by room-temperature sputtering, although, according to X-ray diffraction, they contain an amorphous borosilicate phase.[2] Boron carbide films prepared by DC magnetron sputtering are crystalline only at a silicon substrate temperature above 1210 K.[40] At temperatures < 1210 K, amorphous films are deposited, in which electron diffraction revealed graphite inclusions and short-range ordering.[41,42] Carbon segregations are also assumed to exist in films deposited at 1243 K.[40] Studies[44,45] were technologically biased and dealt with the possibility of using the films and coatings with embedded B_xC for parts of friction units and for enhancing the cutting characteristics.

Specific features of magnetron sputtering of films from targets composed of sintered composites B_xC + (25 mass %, 50 mass % or 75 mass %) TiB_2 have been studied.[36,38,39] Characteristics of films fabricated by RF magnetron sputtering from targets of different composition in the presence and absence of an additional external magnetic field are listed in Table 2. As is seen, the hardness of films in the B_xC-TiB_2 system increases with increasing TiB_2 content (the largest H_V values were observed for the compositions sputtered from the targets containing 25 mass % and 50 mass % TiB_2). These films, like the B_xC film, turned out to be X-ray amorphous. According to X-ray diffraction, film No. 2 was single-phase (a crystal structure of the AlB_2 type, the same as in the case of titanium diboride). The additional magnetic field, which contributes to a higher concentration of ions deposited onto the substrate and, correspondingly, to an increase in the number of crystallization sites and their growth rate, led to an increase in the hardness of both crystalline and amorphous films. It is also noticeable that, in the case of crystalline films, the additional magnetic field favours the decrease in crystallite size and (especially) the narrowing of their size distribution. Sputtering with the use of the additional magnetic field is accompanied by a noticeable reduction of the film roughness. In particular, roughness parameters (R_{rms} is the root-mean-square of the peak heigths at the film, R_{max} is the maximal peak height, R_a is the average peak height) for amorphous film No. 4 (~ 75 mass % B_xC), obtained in the presence and absence of the additional magnetic field, were as follows (nm): $R_{rms} = 0.175$, $R_{max} = 0.75$, $R_a = 0.138$ and $R_{rms} = 0.139$, $R_{max} = 0.7$, $R_a = 0.107$, respectively.

Table 2. Average grain size (L/nm) and microhardness range (H_V/GPa) of the films sputtered in the absence (I) and presence (II) of an additional external magnetic field (~ 0.04 T) from targets of different composition.[38]

Film No.	Target composition (mass %)	I		II	
		L	H_V	L	H_V
1	TiB_2	3.6 ± 1.8	32–39	3.3 ± 1.1	38–42
2	$TiB_2 + 25\,B_xC$	8.5 ± 4.0	36–42	2.9 ± 0.3	46–50
3	$TiB_2 + 50\,B_xC$	amorphous film	44–50	amorphous film	52–57
4	$TiB_2 + 75\,B_xC$	the same	42–48	the same	50–56
5	B_xC	"	36–44	"	42–50

With the use of high-resolution TEM, energy dispersive analysis and Rutherford backscattering spectroscopy, it was demonstrated that applying an additional external magnetic field in the course of magnetron sputtering promotes the nanocrystallization of amorphous films and contributes to the conservation of their composition.[38,39]

3. Bulk materials

Different methods are used for fabricating bulk materials (compacts) based on boron carbide powders. It should be taken into account that, as in the case of other covalent substances (B, Si, Si_3N_4), the covalent character of boron carbide predetermines the high sintering temperature ($> 0.85\,T_m$),[46] *i.e.*, above 2300–2400 K. However, even under these conditions, only hot pressing can lead to formation of samples with low porosity. Recently, the pulsed electric current sintering method has become popular, which allows using preliminarily prepared carbide nano- and micropowders (see, *e.g.*,[47,48]) or, as mentioned above (see Section II.1), synthesized powders.[25,49–52] In this method, the electric current passes through the sintered powder, which is also exposed to a small external pressure. It is assumed that, under these conditions, micro-plasma discharges appear and activate the sintering process, which occurs at considerably lower temperatures and takes much shorter time as compared with hot pressing.[53] Some information on boron carbide materials fabricated by the pulsed electric current sintering method is presented below:

— fully dense samples were obtained by sintering boron carbide powders at 2173 K (t = 6 min, P = 50 MPa); the grain size was 4.05 ± 1.62 μm;[47]

— high-density ultradisperse $Al_2O_3 + 60$ vol.% B_xC composites with addition of up to 5 mass % SiC were fabricated by sintering the powders at 1923 K (t = 4 min, P = 80 MPa); the grain size was 0.55 μm; X-ray powder diffraction revealed small amounts of the $Al_{18}B_4O_{33}$ ($9\,Al_2O_3 \cdot 2\,B_2O_3$) phase in the sintered samples;[48]

— nonstoichiometric B_xC ($x = 3-10$) samples with a relative density of 92% were obtained after synthesis and compaction by the pulsed electric current sintering method at 2173 K (t = 20 min, P = 20 MPa);[51]

— variants of synthesis of B_xC-Al microcomposites (including gradient ones) by the melt infiltration method with the use of pulsed electric current have been described.[50,52]

The fabrication and properties of composites based on the B_xC-TiB_2 system have been well documented (see, *e.g.*,[54–66]). Pseudobinary and more complicated phase diagrams have been studied.[55,57,58,61,64] The eutectic character of the B_xC-TiB_2, $LaB_6-B_xC-W_2B_5$ and $B_xC-SiC-TiB_2$ diagrams has been has been revealed,[55,57,58] although in the last case, the structure of melted samples contained relatively large grains rather than lamellar structures typical of eutectic alloys. Refinement of phase equilibria in the $Ti-Si-B-C$ system with the use of thermodynamic information on the B_xC-TiB_2, B_xC-SiC and $SiC-TiB_2$ pseudobinary sections has shown that no quasi-ternary eutectic forms in the $B_xC-SiC-TiB_2$ system.[61]

The isothermal section of the phase diagram of the $TiB_2-B_{4.5}C$ pseudobinary system, studied as early as in 1966[64] and confirmed by thermodynamic calculations,[61] is shown in Fig. 7. The possible decrease in the eutectic temperature with allowance for the existence of a nanostructure (nanocrystallinity) was estimated using the simplest regular solution approximation. The contribution of excess free energy per mole was written in the form

$$\Delta F = \frac{6V\varepsilon}{L},$$

where V in the volume of 1 mole, ε is the surface energy at the nanograin boundary, and L is the nanograin size.

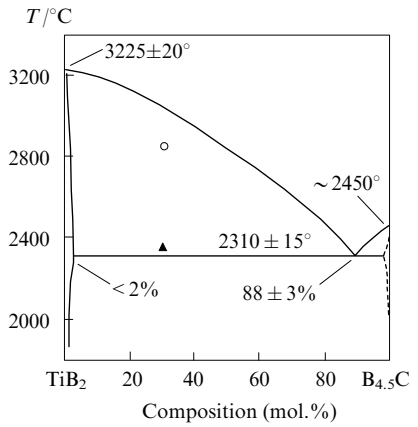


Figure 7. Phase diagram of the $TiB_2-B_{4.5}C$ pseudobinary system.[64]

The decrease in the eutectic temperature is

$$\Delta T_e = \frac{\Delta F}{R \ln x},$$

where R is the gas constant, and x is the maximal boron carbide solubility in titanium diboride at T_e = 2580 K (~2.5 mol.%).[64,67] The results of these calculations for three L and ε values are presented in Table 3. As is seen, a perceptible decrease in T_e is expected at a nanograin size of ~10 nm. It is worth noting that these calculations provide estimates suitable only for determining the upper and lower limits of T_e, which is due to the limitations of the regular solution approximation and the uncertainty in ε values. Nevertheless, such determinations can be useful for estimating the upper limit of operating temperatures of nanocomposites based on refractory compounds, which are used as parts of friction units or as heat-resistant materials.

Table 3. Estimated decrease in the eutectic temperature in nanocrystalline materials based on B_xC-TiB_2 system.[38,68]

ε / J m^{-2}	ΔT_e (K) at L (nm)		
	5	10	50
3	1000	500	100
2	670	340	68
1	340	170	35

Different samples of the B_xC-TiB_2 system have been fabricated by the cast method,[55,59] hot pressing,[56] common sintering (with aluminium additions),[66] pulsed electric current sintering[62,63] and laser processing.[60] The last method (a Nd:YAG laser; power, 500–1000 W; wavelength, 1.06 μm; radiation energy, 120–240 J mm^{-2}; scanning was at a speed of 0.42 mm s^{-1}) yielded eutectic nanostructural surface layers up to 10^3 μm in thickness with a distance of 180 nm between lamellas and a hardness of 32 GPa.

Composite materials based on boron carbide and boron-doped diamond (1.8 at.% B) as cylinders 8 mm^3 in volume were synthesized using a multianvil press at a pressure of 20 GPa and T = 2300 K from turbostratic graphite-like BC_x phases ($x = 1, 1.5, 3$) as precursors.[69,70] The composites exhibited the semiconducting behaviour and extreme hardness (88 ± 3 GPa). The high-pressure behaviour of boron carbide has been addressed in many works (see, *e.g.*,[71–74]). Indentation of this compound led to the phase transition from the crystalline to amorphous state (the estimated transition pressure is 44–49 GPa).[71] An *in situ* Raman spectroscopy study revealed amorphization of B_xC single crystals during unloading to $P \approx 1$ GPa after loading to 50 GPa.[72] However, the pressure *per se* does not lead to amorphization, which was demonstrated by the X-ray diffraction study using the synchrotron radiation source at pressures up to 126 GPa.[73] Density functional theory (DFT) calculations showed that the band gap of boron carbide decreases with increasing pressure, and the metallicity of the compound builds up.[74]

A complex compound based on silicon, boron, carbon and nitrogen is used as a matrix for C(fibres)/SiC(filler)/Si–B–C–N composites, which have a high thermal stability (up to 2000 K).[75] These composites are fabricated

by multiple cycles of melt infiltration of porous preforms composed of carbon fibres and silicon carbide fillers with a Si–B–C–N precursor (followed by pyrolysis).

The above data point to the existence of a rich arsenal of methods of fabrication of boron carbide-based micro- and nanopowders, nanotubes, nanowires, films and bulk materials (see Ref. 1 for a more exhaustive report of fabrication regimes). On the one hand, this shows the large synthetic and technological potential of this compound, and on the other hand, enhances the requirements for choosing an optimal method of fabrication since not only excellent functional properties of such materials but also economic characteristics of their production should be taken into account.

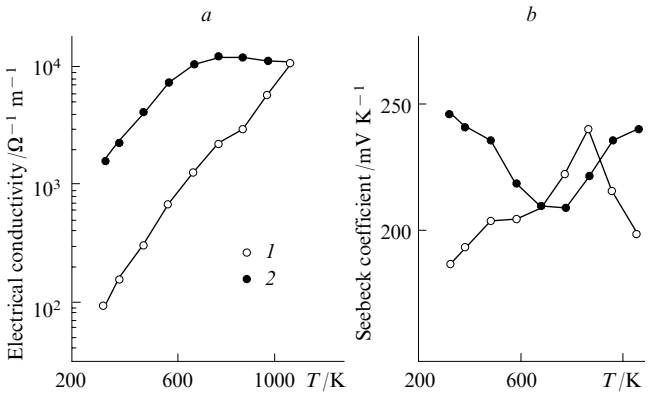


Figure 8. Temperature dependences of electrical conductivity (*a*) and Seebeck coefficient (*b*) of films of ~1 μm in thickness (*1*) and $B_{13}C_2$ bulk samples (*2*).[2]

III. Structure and properties

1. Electronic Structure. Electrical and Optical Properties

As mentioned above, the high hardness, the wide homogeneity range, the transition to the amorphous state and peculiar electrical and optical properties of boron carbide have long attracted the attention of researchers; therefore, it has been addressed in numerous theoretical and experimental studies. If a quite plausible version[18] that B_4C exists as a monoclinic modification with a narrow homogeneity range is taken into account, most information on the synthesis and properties of boron carbide refers to the rhombohedral phase of approximate composition B_xC ($x = 4.25-11.5$). In the literature, these nonstoichiometric compositions are traditionally referred to as B_4C, and only recently some authors have recognized the conventional character of this name and used quotation marks 'B_4C' (see, *e.g.*,[76]) or the designation B_xC emphasizing the nonstoichiometric character of this phase.

Calculations of structural models and electronic structure for crystalline and amorphous boron carbide at different levels of theory have been performed in many studies (see, *e.g.*,[4,42,74,77–80] carried out over the past five years). DFT calculations of the atomic and electronic structures of the crystalline and amorphous boron carbide modifications (using the local-density approximation and the plane-wave pseudopotential method) have shown that the crystal structures exhibit semiconducting properties, while amorphous compositions have semimetallic properties. The pressures of the crystalline phase → amorphous phase transitions have been calculated for different atomic configurations of binding atoms in the boron carbide structure (Fig. 2*a*), and it has been shown that such transitions are accompanied by a decrease in the bulk modulus of the samples.

Considerable attention has been paid to the nature of structural vacancies and the effect of the carbon concentration on the B–C bond character.[77–79] Stable structural vacancies with the localization of electronic states of boron and carbon atoms have been revealed, and this localization leads to the semiconducting nature of boron carbide throughout its homogeneity range.[77] Comparison of first-principles calculation results with experimental data on the enthalpy of formation and infrared phonon modes has shown that a defect model of boron carbide can be suggested: at the carbon content < 13.33 at.%, defects form in the connecting chains, whereas at the carbon content > 13.33 at.%, defects appear in icosahedra.[78] These results correlate with concentration dependences of thermophysical and electrical properties. Calculated hypothetical superhard structures of boron carbide based on $B_{11}C$ icosahedra have been discussed.[79]

Figure 8 shows the temperature dependences of electrical conductivity and Seebeck coefficient of films obtained by the pulsed-ion beam evaporation method and $B_{13}C_2$ bulk samples. As is seen, the films ~1 μm thick at temperatures up to 1000 K have lower electrical conductivity as compared with the bulk samples; however, at 1100 K, these conductivities become equal, which is most likely caused by recrystallization and amorphization processes in boron carbide. The Seebeck coefficient, which also depends on electron–phonon interaction, is a more complicated function of temperature. These data suggested that an increase in the electrical conductivity of boron carbide films (for example, by increasing the substrate temperature or by using an additional annealing) would make their performance in thermoelectric devices more efficient. As applied to the use of boron carbide films as a neutron detector, films obtained by magnetron sputtering at room temperature are recommended.[43]

Photoluminescence spectra of boron carbides of different composition ($B_{4.3}C$, $B_{6.5}C$ and $B_{10}C$, including those with ^{10}B, ^{11}B, ^{12}C and ^{13}C isotopes) have been studied in detail.[81] Analysis of the spectra has demonstrated that the energy of transition from the valence band into the conduction band (E_g) is independent of the chemical (isotope) composition and is close to the E_g values determined from optical and electrical measurements. According to Werheit *et al.*,[81] the electronic structure of boron carbide can be described in the framework of classical band theory concepts but with allowance for defect states.

Raman spectra are often used for monitoring the changes in the boron carbide structure caused by nanoindentation,[71,82] high pressures and electric fields.[72,83–85] Static and dynamic nanoindentation, as well as scratching, are accompanied by the emergence of new bands in Raman spectra at 1330–1350 and 1590 cm^{-1}, which is assigned to structural disordering and possible amorphization. The appearance of carbon and boron clusters has been revealed by Fourier transform IR spectroscopy.[82] The change in the electronic state of carbon atoms (the appearance of sp^2 configurations) has also been reported.[71,82] High-resolution TEM images have revealed the formation of nanocrystals, deformation bands and shears and amorphous inclusions.[71]

Study of the effect of electric fields on Raman spectra showed that, at field strengths < 3000 V cm^{-1}, amorphous carbon clusters are segregated, and in stronger electric fields, sp^2 carbon configurations appear; *i.e.*, the pattern of transformations in boron carbide in electric fields is analogous to that observed under static and dynamic loadings.[83]

2. Mechanical properties

Inasmuch as boron carbide and related composites are used as construction materials, their mechanical properties are actively studied. Table 4 compiles most of recent data on the hardness, flexural strength, crack resistance and elastic characteristics, as well as on the fabrication methods and structural data for boron carbide films and bulk samples. These data show that samples fabricated by hot pressing and pulsed electric current sintering have better properties than the sintered samples. The scatter of results is caused by the high structural sensitivity of mechanical properties and incomplete certification of the objects under consideration. No information is available on the mechanical properties of nanostructural samples with a grain size of ~ 100 nm, not to mention the properties of smaller nanostructures. As noted above (Section II.1), $B_{13}C_2$ compacts with a relative density of 95% and a grain size of ~ 410 nm have been produced by the pulsed electric current sintering method;[25] however, their mechanical properties have not been reported.

Unfortunately, the grain size in crystalline B_4C films with a thickness of 1.3 – 1.5 μm was not reported;[40] however, judging by the hardness and elastic modulus, those films were nanostructural. It is also important that amorphous B_xC films 1 – 2 μm in thickness fabricated by magnetron sputtering with exposure to an additional external magnetic field have high hardness (see Table 2),[38] although the crack resistance, a key parameter for brittle materials, has not been determined for these films.[38, 40] This parameter for all bulk B_xC samples is within 2 – 4 MPa m$^{0.5}$ (see Table 4). The same values are typical of other brittle refractory compounds,[6, 54] for which the major disadvantages are low crack resistance and low thermostability.

To improve these characteristics of boron carbide, numerous studies have been carried out dealing with the effect of additives on the mechanical properties of B_4C-TiB_2,[38, 49, 55–60, 62, 66, 92–94] B_4C-CeO_2,[95] $B_4C-Al_2O_3$,[48] B_4C-BN[96, 97] and B_4C-C [98–100] and other composites. The B_4C-TiB_2 system (Fig. 9) has been studied in most detail. As is seen, the changes in Young's modulus and hardness with an increase in the TiB_2 content are nearly additive, while the changes in fracture toughness and especially flexural strength are nonadditive. The decrease in the strengths of the composites containing > 60 vol.% TiB_2 is attributed to the transformation of the matrix structure to the percolation one. It was shown[92] that the $B_4C-(40-60)$ vol.% TiB_2 composites combine optimal properties, namely, $H_V = 29-30$ GPa, $K = 4.5$ MPa m$^{0.5}$, $\sigma > 800$ MPa and a high electrical conductivity of $\sim 10^6\ \Omega^{-1}$ m^{-1}; *i.e.*, such systems are good candidates for use in abrasive technology (taking into account the possibility of using pulsed electric current sintering in finishing operations and the high operational stability). Further improvement of boron carbide fabrication conditions led to a decrease in the size of B_4C and TiB_2 inclusions to 0.97 and 0.49 μm, respectively; to an increase in hardness to 39.3 GPa, Young's modulus to 497 GPa and flexural strength to 865 ± 58 MPa, whereas the fracture toughness remained at 2.5 – 3.0 MPa m$^{0.5}$ (Ref. 62).

In other studies addressing the mechanical properties of B_4C-TiB_2 composites, analogous strengths and hardnesses have been reported; however, there are some indications that the fracture toughness of 6 – 9 MPa m$^{0.5}$ can be achieved.[49, 66, 93] For B_4C-40 vol.% Al_2O_3 (with SiC additions)[48] and B_4C-4 mass % CeO_2[95] composites, fracture toughness values $K \approx 6$ MPa m$^{0.5}$ have also been found. The

Table 4. Hardness (H_V), flexural strength (σ), fracture toughness (crack resistance /K), Young's modulus (E) and shear modulus (G) of bulk samples and films of boron carbide.

Method of fabrication	Phase composition	Porosity (%)	Grain size L /μm	H_V /GPa	σ /MPa	K /MPa m$^{0.5}$	E /GPa	G /GPa	Ref.
Bulk samples B_xC									
Sintering at 2420 K	B_xC	22	–	21	–	2	–	–	86
Sintering at 2420 K	B_xC	14	14	22	220	2.2	–	–	87
HP at 2170 K	B_xC	1	–	–	675	2.5	–	–	88
Sintering + HIP	B_xC + C traces	~0	~2	~30	392 ± 58	2.7 ± 0.16	454	–	89
HP at 2170 K	B_xC + C traces	5	~3	28.2	363	4.06	420	171	90
PECS at 2020 K	B_xC	0.8 – 4	1.6 – 2.7	25.4 – 27.4	–	3.2 – 3.6	–	–	91
PECS at 2270 K	B_xC	0.5	2.55	~35	~540	~1.7	~570	–	92
B_xC films									
MS with AEMF, $T_s = 420$ K	B_xC	–	see [a]	40 – 46	–	–	–	–	38
B_4C films									
MS with AEMF, $T_s = 300 - 1240$ K	B_4C	–	see [b]	28 – 42	–	–	300 – 470	–	40

Note. The following abbreviations and designations are used: HP is hot pressing, HIP is hot isostatic pressing, PECS is pulsed electric current sintering, MS with AEMF is magnetron sputtering with an additional external magnetic field, and T_s is the substrate temperature.

[a] Amorphous film. [b] Crystalline film at $T_s > 1210$ K.

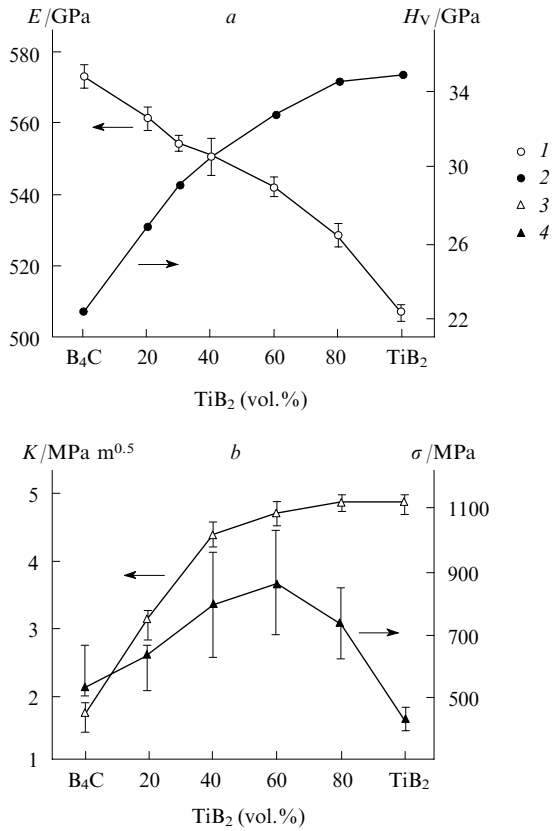


Figure 9. Hardness, and Young's modulus (*a*), fracture toughness and flexural strength (*b*) as a function of composition of the B_4C-TiB_2 system.[92]
All samples had a porosity of 0 %–0.7%; the B_4C and TiB_2 phase size was 0.7–2.6 μm.

mechanism of enhancement of crack resistance in these and other composites is considered to be a result of crack arrest by inclusions (including those formed in interaction between phases). In this context, studies of layered and lamellar boron carbide structures containing additions of boron nitride and multiwall carbon tubes appear in increasing numbers (see, *e.g.*,[96–100]). To fabricate high-hardness textured B_4C samples ($H_V = 38.86 \pm 2.13$ GPa in the direction perpendicular to the crystallographic *c* axis and $H_V = 31.31 \pm 0.79$ GPa in the direction parallel to this axis), compacts obtained by slip casting a powder (HS grade, H C Starck, grain size ~ 1 μm) were exposed to a rotating magnetic field of 12 T with subsequent pulsed electric current sintering ($P = 60$ MPa, $T = 2373$ K, $t = 5$ min).[101] The electric and heat conductivity, as well as elastic characteristics of sintered samples with a relative density of 99% were similar and comparable to analogous properties of B_4C monoliths and single crystals, but the fracture toughness remained at a level of 2.8–3.6 MPa $m^{0.5}$.

The high hardness of boron carbide compacts is known to persist up to 2000 K.[10] However, temperature dependences of mechanical properties and the failure pattern of boron carbide and related composites have been studied to a limited extent (see, *e.g.*,[58, 59, 102, 103]). In flexural tests in the temperature range from room temperature to 1870 K, the strength of compacts made of a mixture of $B_{13}C_2$ and B_4C (with additions of aluminium and Al_2O_3) remains almost unaltered ($\sigma \approx 445$ MPa), and at 1870 K, the transcrystallite fracture changes to the intercrystallite one.[102] The temperature dependence of σ of B_4C-TiB_2 samples with a fibrous composite structure fabricated by crucibleless zone melting is nonmonotonic (the flexural strength decreases at 1070 K and increases with a further increase in temperature to 1670 K).[59] A more or less smooth temperature-induced decrease in σ was observed for eutectic composites $LaB_6-SiC-B_4C-W_2B_5-TiB_2$.[58] The effect of the microstructure of B_4C-, Si-, C- and SiC-based composite materials on their dynamic high-strain-rate behaviour has been discussed.[103]

IV. Conclusions

Analysis of the information on nano- and microsized boron carbide provides the following conclusions.

Many methods of fabrication of boron carbide nano- and micropowders have been developed (direct synthesis from elements, carbothermic and metallothermic synthesis, reactions involving gas-phase precursors and others). As applied to the fabrication of nanopowders, the synthesis from initial amorphous components plays a leading role. Gas-phase methods of production of boron carbide nanowires, nanosheets and nanobelts have also been developed.

Synthesis of nano- and microsized powders is often combined with compaction by pulsed electric current sintering. The latter technology, which makes it possible to reduce the temperature and duration of hot pressing and sintering, is widely used for fabrication of different composites (for example, B_4C-TiB_2, B_4C-CeO_2, $B_4C-Al_2O_3$, B_4C-BN, B_4C-C, B_4C-Al and others). The B_4C-TiB_2 system has been studied in most detail.

Chemical and physical vapour deposition methods are widely used for obtaining and studying predominantly amorphous films based on boron carbide.

By now, a large body of reliable data has been accumulated on the structure, electronic structure and physicochemical and mechanical properties of boron carbide and related composites (although the nature of concentration changes in composite structures, the divergence of results of studying their properties and other facts are still debatable). Unfortunately, this body of information refers mainly to microstructural samples, whereas nanostructures have been occasionally considered. Reliable methods of fabrication of nanostructural compacts have not been developed in detail so far. Special attention should be paid to refining the details of the B–C phase diagram for micro- and nanosized phases.

The nanostructural approach, which turned out to be efficient for creating many new materials,[104] has not met with significant success as applied to boron carbide. A meticulous study of the role of size effects and specific feature of interfaces in physicochemical and mechanical properties of boron carbide-based micro- and nanocomposites will contribute not only to the extension of basic knowledge but also to the extension of application of boron carbide in both traditional areas (polishing, details of friction units, nuclear engineering and armouring) and relatively new areas (high-temperature thermoelectric devices,[2] medical equipment[3] *etc.*). For materials applied in nuclear and space engineering, the use of nanocrystalline boron carbide will help reduce the negative impact of irradiation on these materials, *i.e.*, will mitigate their swelling and radiation embrittlement.[104, 105]

This work was supported by the Russian Foundation for Basic Research (project no. 11-02-92471-MNTI_a) and the Programme of Basic Research of the Presidium of the Russian Academy of Sciences (subprogram P-22).

References

1. A K Suri, C Subramanian, J K Sonber, T S R Ch Murthy *Int. Mater. Rev.* **55** 4 (2010)
2. S Sasaki, M Takeda, K Yokoyama, T Miura, T Suzuki, H Suematsu, W Jiang, K Yatsui *Sci. Technol. Adv. Mater.* **6** 181 (2005)
3. M W Mortensen, P G Sørensen, O Björkdahl, M R Jensen, H J G Gunderssen, T Björnholm *Appl. Radiat. Isot.* **64** 315 (2006)
4. V Domnich, S Reynaud, R A Haber, M Chhowalla *J. Am. Ceram. Soc.* **94** 3605 (2011)
5. R C McCuiston, H T Miller, J C LaSalvia, in *Advances in Ceramic Armor III* (Eds L P Franks, J Salem, D Zhu) (New York: American Ceramic Society, 2008) p. 171
6. R A Andrievski *Russ. Chem. Rev.* **74** 1062 (2005) [*Usp. Khim.* **74** 1163 (2005)]
7. R A Andrievski *Usp. Fiz. Nauk* **177** 721 (2007) [a]
8. R A Andrievski *Usp. Khim.* **80** 890 (2011) [*Russ. Chem. Rev.* **80** 855 (2011)]
9. R A Andrievski *Usp. Khim.* **78** 889 (2009) [*Russ. Chem. Rev.* **78** 821 (2009)]
10. *Neorganicheskoe Materialovedenie. Entsiklopedicheskoe Izdanie. Materialy i Tekhnologii* (Inorganic Materials Science. Encyclopaedic Publication. Materials and Technologies) (Eds G G Gnesin, V V Skorokhod) (Kiev: Naukova Dumka, 2008) Vol. 2, Book 1
11. P S Kislyi, M A Kuzenkova, N I Bondarchuk, B L Grabchuk *Karbid Bora* (Boron Carbide) (Kiev: Naukova Dumka, 1988)
12. *Khimicheskaya Entsiklopediya* (Chemical Encyclopaedia) (Moscow: Sovetskaya Entsiklopediya, 1988) Vol. 1, p. 576
13. F Thevenot *J. Eur. Ceram. Soc.* **6** 205 (1990)
14. R M Mohanty, K Balasubramanian *Key Eng. Mater.* **395** 125 (2009)
15. D Lezhava, G Darsavelidze, D Gabunia, O Tsagareishvili, M Antadze, V Gabunia *J. Solid State Chem.* **179** 2934 (2006)
16. M Beauvy *J. Less-Common Met.* **90** 169 (1983)
17. L B Ekbom, C O Amundin, in *Science of Ceramics* Vol. 3 (Eds R Carlsson, S Karlsson) (Stockholm: Swedish Ceramic Society, 1981) p. 237
18. M Widom, W Huhn, in *Abstract Book of the ISBB 2011, Ankara, 2011* p. 287
19. R McCuiston, J LaSalvia, J McCauley, W Mayo, in *Advances in Ceramic Armor III* (Eds L P Franks, J Salem, D Zhu) (New York: American Ceramic Society, 2008) p. 153
20. A I Kharlamov, N V Kirillova, S N Kaverina *Teor. Eksp. Khim.* **39** (3) 141 (2003) [b]
21. B Chang, B L Gesten, S T Szewczyk, J W Adams *Appl. Phys. A* **86** 83 (2007)
22. S Herth, W J Joost, R H Doremus, R W Siegel *J. Nanosci. Nanotechnol.* **6** 954 (2006)
23. A H Ras, F D Auret, J M Nel *Diamond Relat. Mater.* **19** 1411 (2010)
24. M Kakiage, N Tahara, I Yanase, H Kobayashi *Mater. Lett.* **65** 1839 (2011)
25. S Zhang, W Lu, Ch Wang, Q Shen, L Zhang *Ceram. Int.* **38** 895 (2012)
26. S Chen, D Z Wang, J Y Huang, Z F Ren *Appl. Phys. A* **79** 1757 (2004)
27. J Wei, B Jiang, Y Li, C Xu, D Wu, B Wei *J. Mater. Chem.* **12** 3121 (2002)
28. R Ma, Y Bando *Chem. Phys. Lett.* **364** 314 (2002)
29. M G Rodriguez, O V Kharisova, U Ortiz-Mendez *Rev. Adv. Mater. Sci.* **7** 55 (2004)
30. X Tao, Y Li, J Du, Y Xia, Y Yang, H Huang, Y Gan, W Zhang, X Li *J. Mater. Chem.* **21** 9095 (2011)
31. M Jazirehpour, H-R Bahahrvandi, A Alizadeh, N Ehsani *Ceram. Int.* **37** 1055 (2011)
32. Y Gu, L Chen, Y Qian, W Zhang, J Ma *J. Am. Ceram. Soc.* **88** 225 (2005)
33. U Jansson, J O Carlsson *Thin Solid Films* **124** 101 (1985)
34. S Lee, P Dowben *Appl. Phys. A* **58** 223 (1994)
35. A O Sezer, J I Brand *Mater. Sci. Eng. B* **79** 191 (2001)
36. R A Andrievski, G V Kalinnikov, in *Nanostructured Thin Films and Nanodispersion Strengthened Coatings* (Eds A A Voevodin, D V Shtansky, E A Levashov, J J Moore) (Dordrecht: Kluwer Academic, 2004) p. 175
37. Y Chen, Y-W Chung, S-Y Li *Surf. Coat. Technol.* **200** 4072 (2006)
38. G V Kalinnikov, R A Andrievski, V N Kopylov, D V Louzguine *Fiz. Tv. Tela* **50** 374 (2008) [c]
39. G V Kalinnikov, R A Andrievski, V K Egorov *J. Nano Res.* **6** 89 (2009)
40. V Kulikovsky, V Vorlicek, P Bohac, R Ctvrtlik, M Stranyanek, A Gejneka, L Jadtrabik *Diamond Relat. Mater.* **18** 27 (2009)
41. R Bao, D B Chrisey *Thin Solid Films* **519** 164 (2010)
42. R Bao, D B Chrisey *J. Mater. Sci.* **46** 3952 (2011)
43. R Bao, Z Yan, D B Chrisey *Appl. Phys. Lett.* **98** 192106 (2011)
44. K Jagannadham, T R Watkins, M J Lance, L Riester, R L Lemaster *Surf. Coat. Technol.* **203** 3151 (2011)
45. A Datye, S Koneti, G Gomes, K-H Wu, H-T Lin *Ceram. Int.* **36** 1517 (2010)
46. R A Andrievski *Poroshkovoe Materialovedenie* (Powder Materials Science) (Moscow: Metallurgiya, 1991)
47. S Hayun, S Kalabukhov, V Ezersky, M P Dariel, N Frage *Ceram. Int.* **36** 451 (2010)
48. A K Swarnakar, S G Huang, O Van der Biest, J Vleugels *J. Alloys Compd.* **499** 200 (2010)
49. D M Hulbert, D Jiang, D V Dudina, A K Mukherjee *Int. J. Refract. Met. Hard Mater.* **27** 367 (2009)
50. D M Hulbert, D Jiang, U Anselmi-Tamburini, C Univar, A K Mukherjee *Mater. Sci. Eng. A* **488** 333 (2008)
51. S Zhang, Ch Wang, Q Shen, L Zhang *Adv. Mater. Res.* **66** 25 (2009)
52. T Holland, D M Hulbert, U Anselmi-Tamburini, A K Mukherjee *Mater. Sci. Eng. A* **527** 4543 (2010)
53. A V Ragulya, V V Skorokhod *Konsolidirovannye Nanostrukturnye Materialy* (Consolidated Nanostructural Materials) (Kiev: Naukova Dumka, 2007)
54. R A Andrievski, I I Spivak *Prochnost' Tugoplavkikh Soedinenii i Materialov na ikh Osnove* (Strength of Refractory Compounds and Materials Based on Them) (Chelyabinsk: Metallurgiya, 1989)
55. S S Ordan'yan *Ogneupory* (5) 15 (1993) [c]
56. S Yamada, K Hirao, Y Yamauchi, Sh Kanzaki *J. Eur. Ceram. Soc.* **23** 1123 (2003)
57. S S Ordan'yan, A A Boldin *Ogneupory Tekhn. Keram.* (3) 7 (2005) [c]
58. D D Nesmelov, Candidate Thesis in Technical Sciences, St Petersburg: St Petersburg State University, 2011
59. I Bogomol, T Nishimura, O Vasylkiv, Y Sakka, P Loboda *J. Alloys Compd.* **485** 677 (2009)
60. R M White, J M Kunkle, A V Polatai, E C Dickey *J. Eur. Ceram. Soc.* **31** 1227 (2011)
61. T Ya Velikanova, M A Turchanin, K E Kornienko, A A Bondar, P G Agraval, V V Kartuzov *Poroshk. Metallurg.* (7–8) 11 (2011) [d]
62. S G Huang, K Vanmeensel, O Van der Biest, J Vleugels *J. Eur. Ceram. Soc.* **31** 637 (2011)

63. Ch Xu, Y Cal, K Flodstrum, Zh Li, S Esmaelizadeh, G-J Zhang *Int. J. Refract. Met. Hard Mater.* **30** 139 (2012)
64. E Rudy, S Wenish, J R Hoffman, in *Ternary Phase Equilibria in Transition Metal – Boron – Carbon – Silicon Systems. Report AFML-TR-65-2* Vol. 6, Pt. 1 (Ohio, USA: Metals and Ceramics Division Air Force Materials Laboratory, 1966)
65. M Schouler, M Dicarroir, C Bernard *Rev. Int. Hautes Temp. Refract.* **20** 261 (1983)
66. M Mashhadi, E Taheri-Nassaj, M Mashhadi, V M Sgiavo *Ceram. Int.* **37** 3229 (2011)
67. R A Andrievski *Zh. Vsesoyuz. Khim. O-va im. D I Mendeleeva* **31** (2) 137 (1991) [e]
68. R A Andrievski, G V Kalinnikov *Izv. Akad. Nauk, Ser. Khim.* 1001 (2011) [f]
69. V L Solozhenko, N A Dubrovinskaia, L S Dubrovinsky *Appl. Phys. Lett.* **85** 1508 (2004)
70. V L Solozhenko, A A Kurakevich, N A Dubrovinskaya, L S Dubrovinskii *Sverkhtverd. Mater.* (5) 3 (2006)
71. D Ge, V Domnich, T Juliano, E A Stach, Y Gogotsi *Acta Mater.* **52** 3921 (2004)
72. X Q Yan, Z Tang,L Zhang, C Q Jin, Y Zhang, T Goto, J W Cauley, M W Chen *Phys. Rev. Lett.* **102** 075505 (2009)
73. T Fujii, Y Mori, H Hyodo, K Kimura *J. Phys. Conf. Ser.* **215** 012011 (2010)
74. H Dekura, K Shirai, A Yanase *J. Phys. Conf. Ser.* **215** 012117 (2010)
75. S-H Lee, M Weinmann *Acta Mater.* **57** 4374 (2009)
76. H Werheit, A Leithe-Jasper, T Tanaka, H W Rotter, K A Schwetz *J. Solid State Chem.* **177** 575 (2004)
77. M M Balakrishnarajan, P D Pancharatna, R Hofmann *New J. Chem.* **31** 473 (2007)
78. J E Saal, Sh Shang, Z-K Liu *Appl. Phys. Lett.* **91** 231915 (2007)
79. S Audin, M Simsek *Phys. Status Solidi, B* **246** 62 (2009)
80. V I Ivashchenko, V I Shevchenko, P E A Turchi *Phys. Rev. B* **80** 235208 (2009)
81. H Werheit, H W Rotter, S Shalamberidze, A Leithe-Jasper, T Tanaka *Phys. Status Solidi, B* **248** 1275 (2011)
82. D Ghosh, G Subhash, Ch H Lee, Y K Yap *Appl. Phys. Lett.* **91** 061910 (2007)
83. G Fanchini, V Gupta, A B Mann, M Chhowalla *J. Am. Ceram. Soc.* **91** 2669 (2008)
84. J Guo, L Zhang, T Fujita, T Goto, M Chen *Phys. Rev. B* **81** 060102R (2010)
85. R S Kumar, D Dandekar, A Leithe-Jasper, T Tanaka, Y Xiao, P Chow, M F Nicol, A L Cornelius *Diamond Relat. Mater.* **19** 530 (2010)
86. H R Bavandi, A M Hadian, H Abdizade, N Exsant *J. Mater. Eng. Perform.* **15**280 (2006)
87. H R Bavandi, A M Hadian *J. Mater. Eng. Perform.* **17** 838 (2008)
88. S Yamada, K Hirao, Y Yamauchi, S Kanzaki *J. Eur. Ceram. Soc.* **23** 561 (2003)
89. L Varges-Gonzalez, R F Speyer *Int. J. Appl. Ceram. Technol.* **7** 643 (2010)
90. C Subramanian, A K Suri, T S R Ch Murthy *Barc Newsletter* (313) 14 (2010)
91. D Ghosh, G Subhash, T S Sudarshan, R Radhakrishnan, X-L Gao *J. Am. Ceram. Soc.* **90** 1850 (2007)
92. S G Huang, K Vanmeensel, O I A Malek, O Van der Biest, J Vleugels *Mater. Sci. Eng., A* **528** 1302 (2011)
93. X Y Yue, Sh Zhao, P Li, Q Chang, H Ru *Mater. Sci. Eng. A* **522** 7215 (2010)
94. O Malek, J Vleugels, K Vanmeensel, Sh Huang, J Liu, S Van der Berghe, A Datye, K-H Wu, B Lauwers *J. Eur. Ceram. Soc.* **31** 2023 (2011)
95. Sh-Ch Sun, T Sakamoto, K Nakai, H Kurushita, S Kobayashi, J-Y Xu, H Cao, B Gao, X Bian, W-Y Wu, G-F Tu, S Matsuda *J. Nucl. Mater.* **417** 663 (2011)
96. S Tariolle, F Thevenot, T Chartier, J L Besson *J. Eur. Ceram. Soc.* **25** 3639 (2005)
97. T Jiang, Z Jin, J Yang, G Qiao *Mater. Sci. Eng. A* **494** 203 (2008)
98. F Zhang, Z Fu, J Zhang, H Wang, W Wang, Y Wang *Adv. Mater. Res.* **66** 41 (2009)
99. M Lugovy, V Slyunyayev, V Subbotin, F Liang, J Gou, N Orlovskaya, T Graule, J Kuebler *Ceram. Int.* **37** 2255 (2011)
100. W Lin, N Fang, L He *Adv. Mater. Res.* **152 – 153** 883 (2011)
101. S Grasso, C Hu, O Vasylkiv, T S Suzuki, S Guo, T Nishimura, Y Sakka *Scr. Mater.* **64** 256 (2011)
102. Yu G Tkachenko, D Z Yurchenko, V K Sul'zhenko, G S Oleinik, V M Vereshchaka *Poroshk. Metallurg.* (5 – 6) 60 (2007) [d]
103. S Hayun, M P Dariel, N Frage, E Zaretsky *Acta Mater.* **58** 1721 (2010)
104. R A Andrievski *Osnovy Nanostrukturnogo Materialovedeniya. Vozmozhnosti i Problemy* (Foundations of Nano-structural Materials Science. Potential and Problems) (Moscow: BINOM: Laboratoriya Znanii, 2012)
105. R A Andrievski *Ros. Nanotekhnol.* **6** 34 (2011) [h]

[a] — *Physics-Uspekhi (Engl. Transl.)*
[b] — *Theor. Exp. Chem. (Engl. Transl.)*
[c] — *Retract. Tech. Ceram. (Engl. Transl.)*
[d] — *Powder Metall. Met. Ceram. (Engl. Transl.)*
[e] — *Mendeleev Chem. J. (Engl. Transl.)*
[f] — *Russ. Chem. Bull., Int. Ed. (Engl. Transl.)*
[g] — *J. Superhard Mater. (Engl. Transl.)*
[h] — *Nanotechnol. Russ. (Engl. Transl.)*